

Article

Chemically Oscillating Reactions as a New Model for the Formation of Mineral Patterns in Agate Geodes and Concretions

Dominic Papineau

London Centre for Nanotechnology, Department of Earth Sciences, and Centre for Planetary Science, University College London, London WC1H 0AH, UK; d.papineau@ucl.ac.uk

Abstract: Agate geodes contain spheroidal patterns characterized by spectacularly coloured and circularly concentric laminations with radially aligned quartz crystals, yet the origin of these geometric patterns has remained enigmatic. Here, detailed comparisons are documented between these kinds of patterns in a selection of geodes and concretions and those produced by abiotic chemically oscillating reactions. We find strikingly comparable self-similar, fractal patterns in both natural volcanogenic geodes and sedimentary concretions as well as in these benchtop experiments. In addition, the mineralogical composition of patterns and associated organic matter point to the oxidation of organic compounds in both geodes and concretions. This process occurred during diagenetic or supergene alteration, and it is consistent with spontaneous and abiotic chemically oscillating reactions. It is concluded that the oxidation of organic acids was involved in the formation of these patterns and that these rocks indicate oxidation–reduction reactions involving organic carbon, which itself may be abiotic or biological in origin. Hence, agate geodes and concretions represent the abiotic biosignatures of possible biological origin in volcanic and sedimentary rocks.

Keywords: abiotic; biosignature; origin of life; concretion; agate geodes



Citation: Papineau, D. Chemically Oscillating Reactions as a New Model for the Formation of Mineral Patterns in Agate Geodes and Concretions. *Minerals* **2024**, *14*, 203. <https://doi.org/10.3390/min14020203>

Academic Editors: Magdalena Dumańska-Słowik, Jens Götze, Tomasz Powolny and Panagiotis Voudouris

Received: 13 November 2023

Revised: 5 January 2024

Accepted: 2 February 2024

Published: 16 February 2024



Copyright: © 2024 by the author. Licensee MDPI, Basel, Switzerland. This article is an open access article distributed under the terms and conditions of the Creative Commons Attribution (CC BY) license (<https://creativecommons.org/licenses/by/4.0/>).

1. Introduction

The origin of agate geodes and the characteristic geometric patterns they contain are enduring problems of geology [1–3]. The enigmatic origin of circularly concentric and equidistant laminations in agate geodes is particularly emblematic of the complexity of this scientific problem [1]. The same kinds of concentric equidistant laminations, each with their own colour-intensity gradient, also occur in botryoidal minerals [4,5]. These self-similar rounded and concentric structures have an equivocal origin, but they have been suggested to form through diffusion processes [2]. Objects such as geodes and concretions differ primarily by their occurrences in different rock types. Agate geodes most often occur in volcanic rocks that can either be SiO₂-poor such as andesite and basalt or SiO₂-rich such as rhyolite and rhyodacite [3]. Concretions dominantly occur in sedimentary rocks that can be siliciclastic, such as mudstone and sandstone, or chemically precipitated sedimentary rocks such as carbonate, chert, banded iron formation, and phosphorite. Moganite is also commonly associated with chalcedonic quartz forming macroscopic patterns in geodes. However, no specific processes have been identified to produce the radial orientation of chalcedony fibres, their twisted growth structures, nor the circular concentricity of laminations, their colour gradients, and the cavity structures they produce through spherical twinning (Figure 1a,b).

In comparison, concretions are also macroscopic, ellipsoidal (or sub-spheroidal), and rocky objects, but these occur in sedimentary rocks throughout the geological record. They start forming quickly during burial, within weeks to years and near the sediment–water interface and involve metabolically distinct microbial populations that are not distributed evenly inside concretions [6,7]. Perhaps most notably, concretions contain an exceptional archive of animal and microbial fossils (e.g., Figure 1c,d) that make them critically important

to understand biological evolution throughout Earth history [8–11]. Some concretions also have perfect rounded laminations of variably coloured minerals (e.g., Figure 1e,f) and are they commonly displayed in museums and sold in ‘rocks and minerals’ shops around the world. However, the processes involved in their formation and their significance for fossilisation remain obscure. This problem is therefore indistinct from that of the origin of patterns in agate geodes, since they exhibit many common characteristics, and especially the common occurrence of organic matter and of self-similar patterns of concentric equidistant laminations inside both these spheroidal rocks.

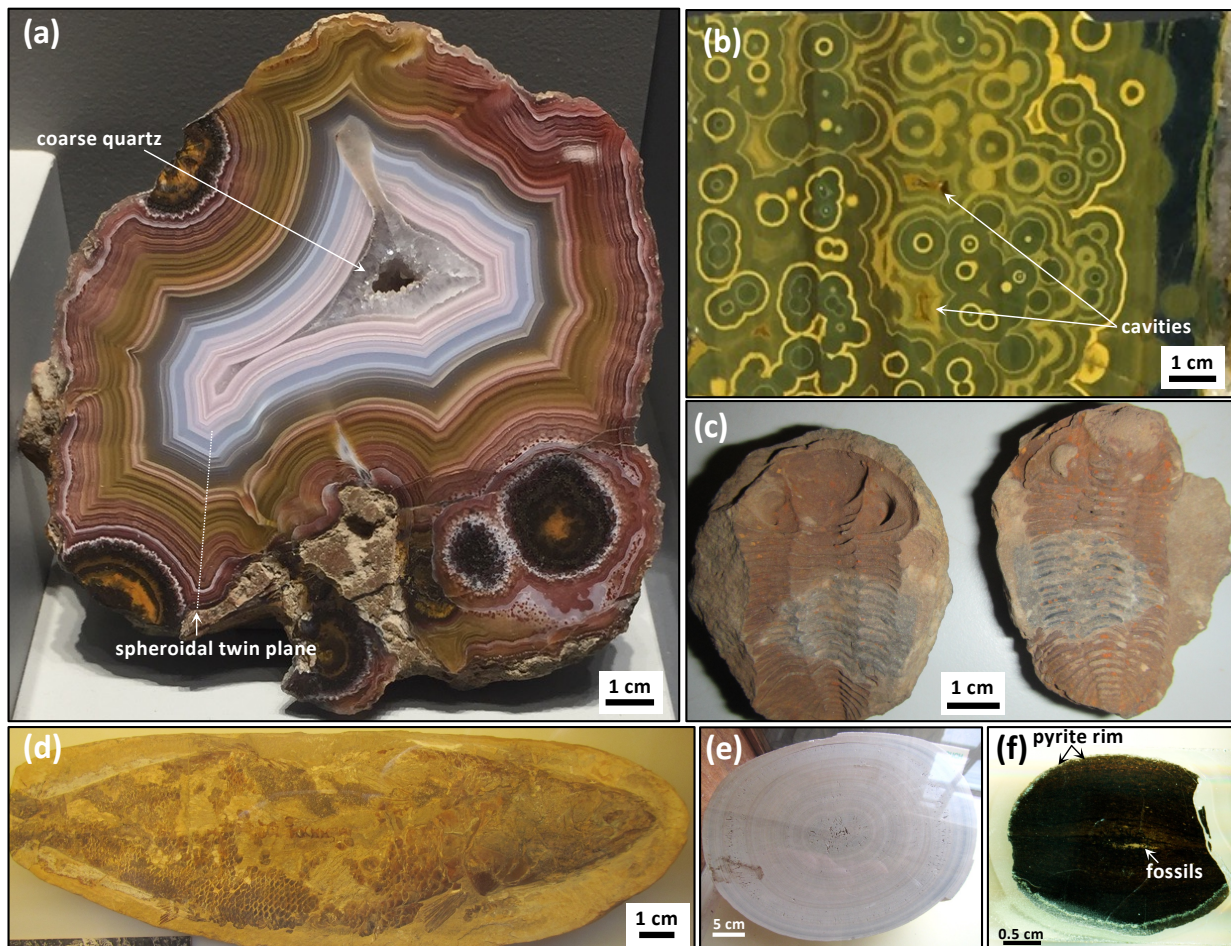


Figure 1. Examples of agate geodes and fossiliferous concretions. (a) Sub-spheroidal geode from Laguna Ranch, Chihuahua (Mexico), showing a cavity lined with coarse-grained, inward-pointing and acicular quartz crystals and spheroidal twins. (b) Agate geode from an unknown locality showing self-similar patterns with a proliferation of circularly concentric spots, twinning, cavities and colour gradients. (c) Trilobite fossils inside proportionally sized ferruginous limestone concretion from Bolivia. (d) Fossil fish inside proportionally sized limestone concretion from the lower Cretaceous of Brazil. (e) Circularly concentric limestone concretion from an unknown locality. (f) Organic-rich cherty concretion with a pyrite rim (arrow) and fossiliferous core from the Doushantuo Formation (Member II).

The lack of an adequate model to explain why concretions and geodes often preserve organic matter and distinct morphologies such as circularly concentric laminations, spheroidal twins, and radiating acicular crystals has been an impediment to biosignature and exobiology research. This is because many key ancient fossils are preserved with botryoids or within concretionary structures, including Earth’s oldest fossil microorganisms from the Eoarchean–Hadean Nuvvuagittuq Supracrustal Belt [12,13]. These are filamentous microfossils that co-occur with rosettes and granules, composed of quartz and haematite,

and that occur inside jasper concretions. Concretions are known to include fossil biomass or organic matter, and, therefore, it is natural to hypothesize that organic matter decay might be involved in their formation [8]. This is distinct from agate geodes, however, which often contain organic matter [14,15], but no fossils, to the knowledge of the author, and which usually occur in volcanic rocks instead of sedimentary rocks for concretions. Yet, the variable occurrence of organic matter within agate geodes and concretions requires an adequate explanation with predictive capability. The proposed explanation for concretion formation when they host fossils located in their geometric centre typically involves some 'secondary' (i.e., diagenetic or post-depositional) nucleation process around a core of biomass and later replacement during silicification, calcification of carbonate and phosphate, or pyritization. However, this explanation is partly nebulous in terms of what was the initial phase that was replaced, what secondary processes were involved during nucleation and mineralisation, and how was organic matter related to the formation of associated 'diagenetic spheroids'? Diagenetic spheroids are rocks formed during diagenesis with a rounded, sub-spheroidal morphology as well as microscopic to macroscopic circular patterns. This new terminology is used here to propose a new connection between agate geodes and concretions, tentatively grouped under this umbrella. This is because the above archaic model also does not explain the patterns of concentric equidistant laminations and mineral compositions and, as a result, the reason why concretions exhibit distinct sub-spheroidal morphologies has often been ignored or left unexplained.

This contribution highlights key chemical, mineralogical, and morphological similarities between the patterns and compositions produced by chemically oscillating reactions (COR) and those of the enigmatic self-similar patterns in agate geodes and concretions. First, a brief background is presented on the new hypothesis that COR might play a role in the formation of concretions and agate geodes. Then, this is followed by new optical and micro-Raman analyses of two specimens with internal self-similar patterns: a late Devonian carbonate-rich agate geode and an agate geode with red ferruginous limestone from an unknown age and locality. The discussion then explores the importance of concretions and geodes in the carbon cycle and in the geobiological record. If COR are involved in the formation of agate geodes and concretions, they could be crucial for exobiology, as they can be predicted to link abiotic carbon cycling with pattern formation and the spontaneous oxidation of organic matter, especially of carboxylic acids, as well as to lead to new avenues about the biosignatures of past extraterrestrial life.

2. Background on Chemically Oscillating Reactions

Chemical oscillations can spontaneously occur under standard conditions and can involve the oxidation of carboxylic acids by strong oxidizers, such as oxidized halogens, and strong acids like sulphate or hypophosphite [16,17]. When catalysed with redox-sensitive ferroin (phenanthroline ferrous sulphate), COR produce notable and characteristic fractal patterns [18] displayed as circularly concentric equidistant waves that radially expand from randomly located spots over minute time scales. Eventually, COR produce sub-millimetre size carbon dioxide bubbles attached to the Petri dish. The ring-shaped waves develop gradients of blue–grey colours that represent the oxidized ferroin, which is ferrous in the orange-coloured initial solution, and they destructively interfere together to form twins and cavity-like structures. Interestingly, rare earth element dyes are often used in COR instead of ferroin, and the source of organic molecules can include a range of carboxylic acids and ketones, whereas the strong oxidants can also be interchanged between NaBrO_3 , NaH_2PO_2 (hypophosphite), Mn-sulphate, and hydrogen peroxide [16,17]. During the chemical oscillations, electrons are transferred to more electronegative and oxidised anionic groups and produce energy through an electromotive force that diffuses reaction products such as Fe^{3+} and halogenated carboxylic acids. Because these intermediates can be cyclically re-reduced and re-oxidised, the radially diffusing patterns are self-similar as they develop over several size dimension scales; hence, COR produce fractal patterns. COR are thus spontaneous, abiotic, out-of-equilibrium, and redox reactions that produce

characteristic self-similar patterns and carbon dioxide from the oxidation of carboxylic acids with sulphate and oxidised halogens.

The reactants of COR are all relatively common in some diagenetic environments, and because of their high solubilities (especially those of sulphate, bromate, and iodate), they can be naturally concentrated during the diagenetic dehydration of sediments, such as in evaporitic environments. The variability of oxidation states in halogen elements is key and it is exploited in various COR because the reactions produce patterns when the reduced halogen salt, such as bromide or iodide, is mixed with oxidized halogen, either bromate or iodate. When biomass decays during putrefaction, the pH of diagenetic pore solutions can increase to highly alkaline and ammoniated solutions during early decomposition [19], which enables silica to be soluble and form colloids, to decreasing alkaline solutions as diagenesis progresses and with the increase in sulphide and CO₂ produced by microbial processes such as anaerobic heterotrophy and sulphate-reduction. These processes can lead to the accumulation of diagenetic pore water silica, phosphate, bicarbonate, and sulphide [20]. Hence, there are similarities between biological respiration and abiotic COR, and these processes are expected to take place during diagenesis, when biomass decomposes, and have previously been argued to be preserved in association with concentric waves around decayed biomass, deflecting earlier sedimentary laminations, and forming spheroidally layered mineral patterns such as in botryoidal quartz and malachite [4,5,21,22]. To test this COR model on agate geodes, the relevant types of pattern morphologies produced by a large number of COR experiments (> 250) need to be documented and then compared to the self-similar patterns displayed by agate geodes and concretions. Beyond the patterns inside these objects (Petri dish vs. rocks), this work also compares the substances of new COR experiments with those substances in geodes and concretions, such as inclusions of organic matter and mineral compositions using correlated microscopy with micro-Raman spectroscopy.

3. Materials and Methods

3.1. Chemically Oscillating Reactions

The new COR experiments are performed in 10 cm diameter Petri dishes using the following reactants: 6 mL of (1 M) NaBrO₃ mixed with (0.33 M) H₂SO₄, 1 mL of (1 M) malonic acid, 0.5 mL of (1 M) NaBr, 1 mL of (25 mM) Ferroin (phenanthroline ferrous sulphate) and a drop of dilute triton X-100 soap [18]. The first three solutions are mixed until the yellow colour disappears, which takes approximately two minutes of gentle stirring (this is when the most bromine gas is released, perceptible from its odour). The ferroin redox indicator and dilute soap are then added. A bicolour orange–blue spontaneously forms upon contact of the ferroin with the solution. If the solution is then stirred again, the homogenized colours will oscillate between orange–red to blue–purple–grey. Some dark microscopic precipitates sometimes form. If the homogenous solution is left still, visibly contrasting chemical waves of perfectly circular concentric rings randomly appear and expand radially, and periodically repeats over second to minute times scales. All experiments are performed under uncontrolled standard conditions often in a hood, although vibrations and air currents in the latter affect pattern formation; hence, experiments are often performed on a benchtop after the degassing of bromine gas in the hood. No experiments reported have patterns triggered with a tool, which can indeed trigger pattern formation. After various trials, it is found that a white LED light bench works best to visualise the characteristic COR patterns in transmitted light. The reactions are spontaneous and out-of-equilibrium, and the pattern development lasts between about 30 and 45 min, depending on the number of resets.

3.2. Geological Specimens and Optical and Micro-Raman Analyses of Patterned Agate

Images of centimetre- to decimetre-size agate geodes were collected using a document scanner with 1200 ppi resolution, after cutting with a diamond saw and polishing to an optical finish with 0.25 µm alumina. Concretions were photographed using a CCD camera.

The first specimen was obtained from Mt Lyall in Québec, an Appalachian mountain famous for its agate geodes. Lyall geodes are common in volcanic rocks of the York River Formation, interbedded between lower Devonian sedimentary strata [23]. However, the precise sample location is not known as the specimen was procured from a private collector. Similarly, the red limestone agate geode from unknown locality was also purchased from a dealer. A BX-51 Olympus petrographic microscope located at UCL was used to collect reflected light images on polished rock slabs with the following objectives: 5×, 10×, 20×, 50×, and 100×. A few reflected plus transmitted combo light images were also collected. No oil immersion or ink markings were used on the polished thin sections (0.25 µm Al₂O₃ last step).

Micro-Raman was then performed with the α300 WITec confocal laser scanning micro-spectroscopy system in the Geological Spectroscopy Laboratory at UCL, using a 532 nm laser set at 7 or 8 mW. The WITec α300 Raman system was used to image organic matter located in the geometric patterns of agate geodes. An optic fibre of 50 µm in diameter was the pinhole used to collect inelastically scattered photons in confocal planes within one micron of the surface. The reflected inelastically scattered photons were first filtered by a notch filter and then dispersed through a 600 lines/mm grating in the spectrometer, before being collected on an electronically cooled CCD detector, which provided a spectral resolution of about 4 cm⁻¹ over a bandwidth of about 4000 cm⁻¹. The spatial resolution was set at one pixel per two microns to three pixels per micron, whereas the acquisition time on each pixel was 0.4 to 0.6 s. Raman spectra shown were generated from regions of interest selected based on identical relative intensities and spectral peaks and processed with the WITec Four Plus software.

4. Results

4.1. Patterns in Chemically Oscillating Reactions

By far the most common patterns in experiments (more than 50%) are the circularly perfect, self-similar, equidistant oxidation spots with merging chemical waves that form cavity-like structures (Figure 2a–e). Initially, COR experiments show dozens of circularly concentric, millimetre-sized spots that grow into circularly concentric centimetre-sized spots, and eventually into decimetre-sized spots (Figure 2a). When two circular waves from two distinct oxidation spots come in contact, a process of destructive interference occurs and forms circular twins and cavity patterns (Figure 2b). When this occurs from two oxidation spots and with many successive waves, a twin plane forms, whereas the destructive interference eventually forms cavity structures when twins arise from multiple oxidation spots (Figure 2b,c). As the COR progresses, the circularly concentric waves diffuse radially and display stronger colour gradients (Figure 2c). In some experiments, circularly concentric waves display imperfectly equidistant laminations and even mixed chaotic patterns that can lead to stromatolite-like columnar elongated structures, although the self-similarity of the patterns is preserved in all cases (Figure 2d).

Eventually, the chemical waves fill the entire Petri dish with a homogeneous blue colour and the experiment can be reset by gentle stirring to produce another generation of similarly shaped spots compared to the previous generation, but not at identical locations. It is in the late reaction stages that spirals and tightly packed laminations develop although cavities and twins persist until the end (Figure 2e). The self-similar patterns change from one experiment to another, but no specific location can be predicted to become oxidation spots. Presumably, the system is highly sensitive to initial conditions. In several experiments, a spotted zebra-stripe or arborescent types of patterns oscillate in the background with a different, faster, second-order time period. However, these are distinct from the first-order chemical oscillations displayed as the discrete oxidation spots described above. Hence, the oscillations in the blue and orange colours are represented by at least three orders of time periods: a first-order of pattern formation with sub-millimetric to decimetric oxidation spots with chemical waves that have periods in the order of about 30 to 90 s, a second order of pattern formation with spotted, arborescent, or inverted patterns that have

periods in the order of 10 to 20 s, and lastly a third order of patterns, completely filled with blue and resetting to an orange background, which thus represent a third-order of chemical oscillations with periods on the order of 25 to 35 min.

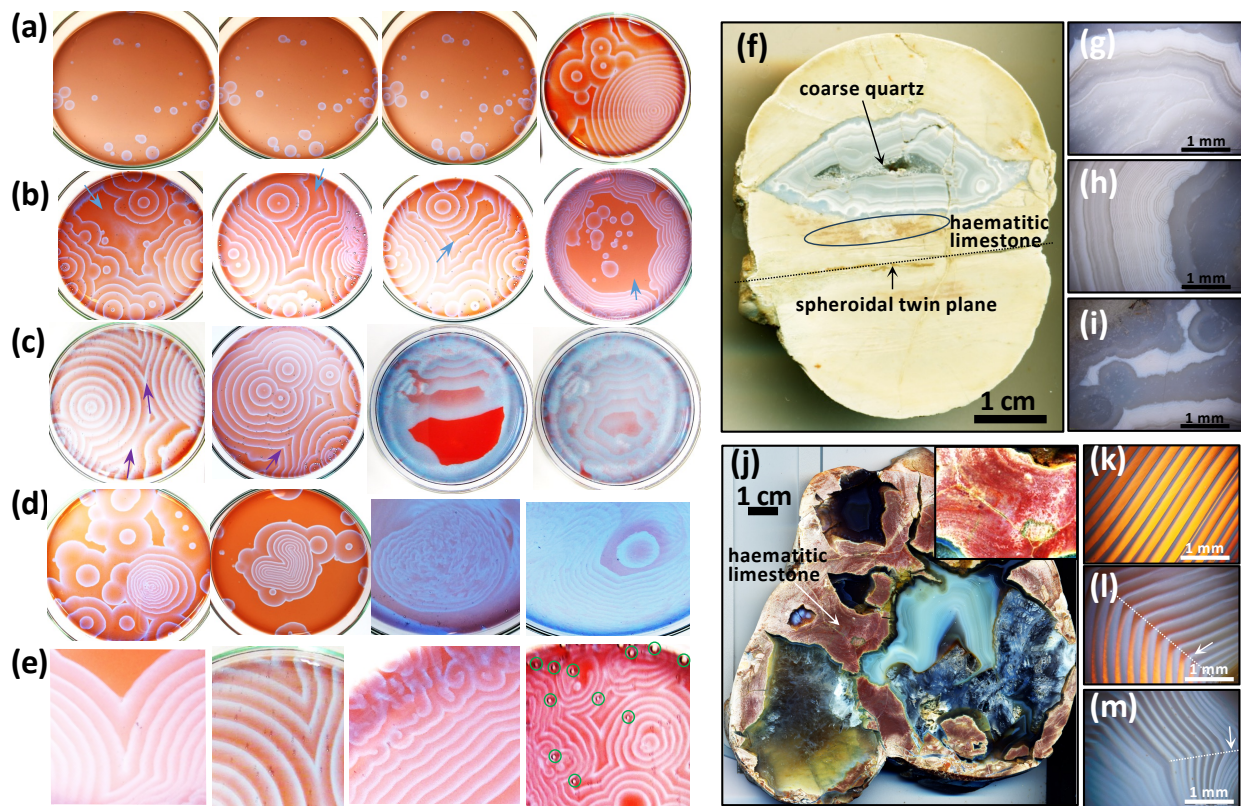


Figure 2. Morphological comparison of sub-millimetric to decimetric self-similar patterns in COR ((a–e), transmitted light images of COR with orange–blue coloured solution in one decimetre diameter Petri dishes) and in an agate geode and agate-bearing concretion (f–h). In COR experiments, none of the patterns were induced. (a) Randomly localised oxidation spots spanning four orders of magnitude in size dimension, (b) cavity shapes (blue arrows) with imperfect to perfect circularly concentric waves, (c) decimetre-sized structures of oxidizing spot and cavity shapes associated with twins (purple arrows) and strong colour gradients, (d) centimetre-sized imperfectly circular spots with imperfectly equidistant laminations or mixed-chaotic pattern of lines, (e) zoomed-in views of twins, nearly perfect equidistant laminations, spirals, and multi-lined cavities. In all experiments, the small spherical bubbles contain the CO₂ produced during the reaction (green circles in (e)). (f) Reflected light image of a spheroidally twinned agate geode from Mt Lyall showing a central cavity with coarse quartz adjacent to brown–orange coloured haematitic limestone. (g–i) Circularly concentric laminations with brown colour gradients inside the cavity. (j) Reflected image of an agate geode from unknown locality with equidistant laminations of SiO₂ polymorphs near the geode centre and red–pink coloured haematitic limestone. (k–m) Reflected and transmitted light images (combo on one-centimetre-thick slab) of these equidistant laminations showing parallel alignment, circular concentricity, colour gradients, and twins (white dotted lines).

4.2. The Optical Analyses of Patterns in Agate Geodes

Notable patterns in agate are self-similar, with a nearly perfect geometry (Figure 2f). They form parallel-aligned laminations, circularly concentric spots and laminations, colour gradients, spherical twins, and cavity structures (Figure 2g–i). They are typically located near the geometric centre of the geode (Figure 2f), and the pattern also consists of circularly concentric equidistant laminations that occur inside a cavernous cavity lined with coarse quartz with a euhedral-prismatic habit (Figure 2f). The studied Mt Lyall geode is also spheroidally twinned and contains patches of orange–brown haematitic limestone. The

concentric spheroidal laminations occur up to the central part of the cavity and the quartz laminations are coloured white, brown, and in shades of grey (Figure 2g–i). The circularly concentric equidistant laminations also form spheroidal structures linked to sub-linear lamination by spheroidal twins (Figure 2i). In the red limestone agate geode, there are multiple agate compartments (Figure 2j), and the agate cavity structures commonly contain equidistant laminations that display variable colour gradients, twin planes, and circular to linear concentricity (Figure 2k–m). The different agate compartments are linked by septarian red-coloured crack structures of haematitic limestone that constitute the geode and which also exhibit patterns of cavity structures (Figure 2j—inset).

4.3. The Raman Analysis of Minerals Associated with Organic Matter in Agate Geodes

Regions in the Mt Lyall agate geode and in the red limestone agate geode were selected for Raman hyperspectral imaging based on the presence of brown colour gradients, circular concentricity, and spheroidal twins (Figures 2g–i and 3a). The objective was to determine whether there is a petrographic correlation between these patterns and the petrographic distribution of organic matter and carbonate.

Firstly, for the Mt Lyall agate geode, micro-Raman imaging reveals that quartz dominates the matrix of twinned circularly concentric spots with a single strong peak at 469 cm^{-1} , whereas moganite is also co-occurring with quartz and twinned circularly concentric laminations with an additional weak peak at 504 cm^{-1} (Figure 3b–f). Myriad micron-sized crystals of calcite dominantly occur in the quartz with peaks at 1090 cm^{-1} (Figure 3d). These often occur in direct association with micron-sized disseminations of organic matter (OM), which are also specifically concentrated in the geometric centre of quartz–moganite circularly concentric structures (Figure 3c). The Raman spectrum for OM, deconvoluted with Lorenz functions, shows the following peaks: D1 at 1346 cm^{-1} , D2 at 1620 cm^{-1} , D3 at 1530 cm^{-1} , D4 at 1245 cm^{-1} , G at 1606 cm^{-1} , and finally a possible D5 peak at 1453 cm^{-1} (Figure 3g).

Secondly, for the red ferruginous limestone agate geode, micro-Raman imaging shows the presence of myriad micrometre- to nanometre-sized mineral inclusions in quartz and moganite that compose the fractal patterns of cavity-like structures (Figure 4a–f). These mineral inclusions are composed of two types of OM, which are primarily distinguished by different G-band positions, respectively, at 1572 cm^{-1} and 1599 cm^{-1} (Figure 4g). There are also two types of carbonate minerals that include calcite with a peak at 1090 cm^{-1} and a possible dolomite with a peak at 1099 cm^{-1} , but also a sharp and strong peak at 549 cm^{-1} . The latter peak occurs in a region of metal–oxide peaks; however, this identification is unclear. Other micrometric- to nanometric-sized mineral inclusions include anatase with a strong peak at 145 cm^{-1} and a medium–weak peak at 632 cm^{-1} , cristobalite with peaks at 418 and 230 cm^{-1} , and lastly another unknown phase associated with quartz with peaks at 574 and 632 cm^{-1} , possibly from metal–oxide bonds (Figure 4g).

4.4. Characteristic Patterns in Concretions

Concretions possess several patterns and substances similar to those described for agate geodes above (Figure 5, right column). For instance, concretions can occur as spot proliferations in sedimentary beds and can display a multitude of circularly concentric layers. Metre-sized concretions can also exhibit twins, cavity structures, and colour gradients, as well as radially aligned patterns. For substances, concretions can be darkened (brown to black) by enrichments of organic matter, reddened (orange to red brown) by gradients of ferric to ferrous iron oxide minerals, or yellowed by the presence of circularly concentric layers of pyrite. Concretions also almost ubiquitously contain some carbonate and iron oxides.

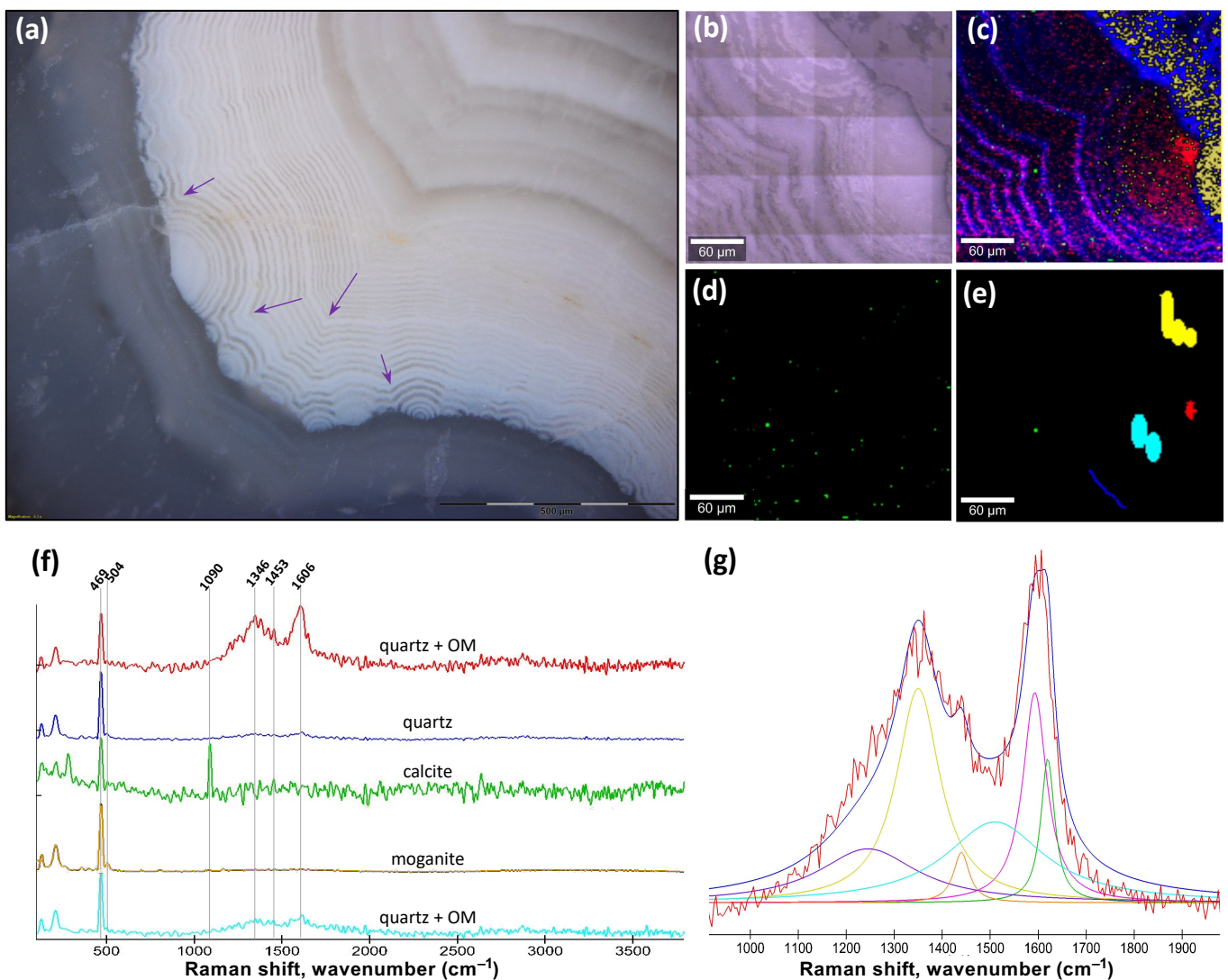


Figure 3. Hyperspectral analysis of Mt Lyall agate geode in Figure 2f. (a) Reflected light image inside the cavity showing circularly concentric spots with twins (purple arrows) and brown coloured gradients. (b) Reflected light image of a twinned spheroid selected for Raman hyperspectral imaging and showing perfect circularly concentric hemispherical spots about 100 μm in diameter equidistant laminations in the concretionary cavity showing. (c) Raman hyperspectral images of quartz in two different orientations (black and blue), quartz with OM (purple), quartz with a central concentration of OM (red), moganite (yellow), and micron-sized calcite crystals (green). (d) Hyperspectral image only for the calcite peak at 1090 cm^{-1} . (e) Regions of interest for pixels selected to extract Raman spectra shown in (f), with correlated colours. (f) Raman spectra of the phases detected and representing averages of selected coloured pixels in (e). (g) Raman spectrum of the OM modelled with six Lorentz-fitted functions: purple is the D4 peak, yellow is the D1 peak, orange is the 1453 cm^{-1} peak, turquoise is the D3 peak, purple is the G-peak, and green is the D2 peak. Correlation coefficient R^2 is 0.987 between the measured spectrum (red) and the modelled spectrum (blue). The colours in the Raman hyperspectral images correspond to colours of these Raman spectra.

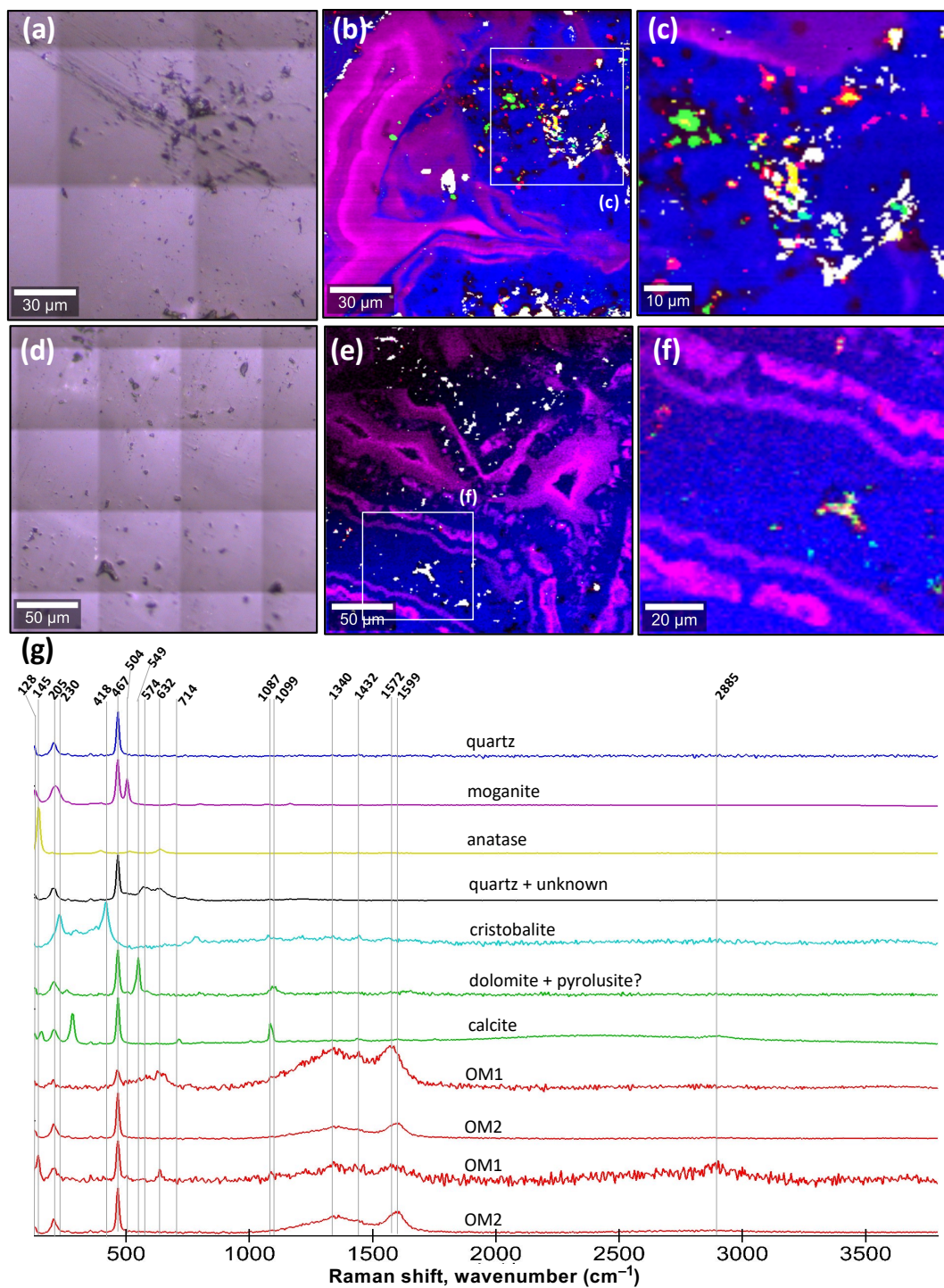


Figure 4. Raman analysis of the unknown agate geode in Figure 2j. (a) Reflected light image of a well-polished quartz region with a cavity structure and black-coloured grains for mineral inclusions. (b,c) Raman hyperspectral images of quartz and moganite (blue and purple) with inclusions of organic matter (red), carbonate (green), anatase (yellow), and OM mixed with carbonate and quartz (white). There are two types of organic matter (OM1 and OM2) and two types of carbonate (calcite and dolomite). Cristobalite (turquoise) is common, and where OM co-occurs with carbonate and anatase, the colour is white. (d) Reflected light image of another well-polished region of quartz with several cavity structures and black-coloured mineral inclusions. (e,f) Raman hyperspectral images of quartz and moganite with inclusions of organic matter closely associated with carbonate, anatase, and cristobalite. (g) Raman spectra of phases detected in these two regions and identified based on the major or unique characteristic peaks.

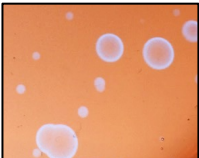
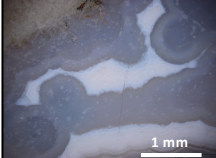
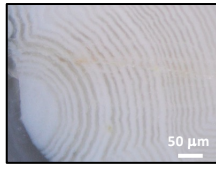
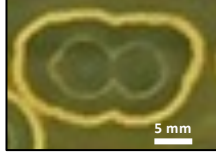
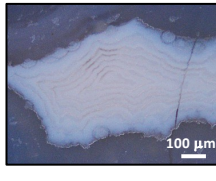
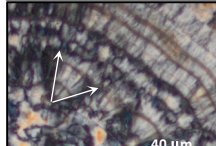
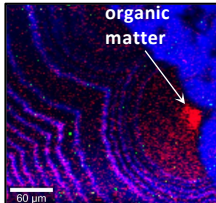
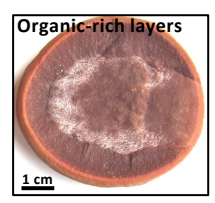
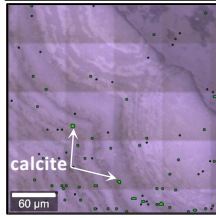
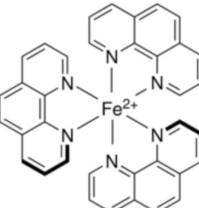
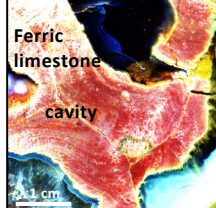
	Objects:	COR	Agate geodes	Concretions
Patterns	Spot proliferations			
	Circular concentricity			
	Twins			
	Cavity structures			
	Colour gradients			
	Radiations	 		
Substances	Organic reactants	<chem>OC(=O)CC(=O)O</chem>		
	Carbonate products			
	Fe catalyst			

Figure 5. Summary of comparisons between patterns and substances observed in agate geodes and COR. All photos from the author, except the molecular structures from Wikipedia.

5. A Discussion on the Morphology of Self-Similar Patterns in Agate

5.1. Abiotic and Biological Growth Models for Agate Geodes and Concretions

The following section describes some previously proposed models for the formation of agate geode and of concretions. First, some previously proposed crystallization mechanisms shall be considered alongside pattern formation. Oscillations over at least five orders of size dimension, from hundreds of nanometres to centimetre scales, have been described to form the self-similar fractal patterns in agate geodes [24]. Within their radial patterns, the elongation direction of chalcedony fibres in agate geodes is typically down the [110] crystallographic direction as opposed to prismatic quartz crystals, which grow down the [001] direction [25]. The acicular-fibrous chalcedony in radial quartz is also twisting as a screw dislocation about [110], which yields an oscillating fibre growth direction down the *c*-axis [24]. These geometric patterns underlie a specific process of mineralization. A model based on Ostwald's rule, which is that when a substance changes from one state into another state, the favoured state it will adopt is the one nearest in stability to the original state [26], can also be considered. Mineralisation sequence from colloidal silica to cristobalite, and then onto moganite and cryptocrystalline or chalcedonic quartz, is usually suggested based on detailed petrographic observations [1]. It can then be understood that the favoured phase to form from a process resulting in crystallisation has been explained based on the irreversible thermodynamics of the crystal structure. In Palaeoproterozoic agates from the Ludikovi Group in northwest Russia, the mineralisation of quartz was demonstrated to be strongly influenced by the abundance of organic matter [14]. The crystallisation of quartz has also been proposed to proceed from inside towards the outside edge, along with co-diffusing substances that eventually reach saturation and remain preserved as bands [1].

The Liesegang diffusion phenomenon called "banding" is known to occur in gels and is proposed as a possible diffusion mechanism to explain patterns exhibited by natural agates from volcanic terrains [2]. For instance, Liesegang experiments are known to produce periodic banding as well as dendritic patterns when a substance of a higher density and viscosity diffuses through another with a lower density and viscosity, which has been explained by the processes of viscous fingering and diffusion-limited aggregation [27]. However, the Liesegang diffusion phenomenon is not known to specifically involve reactions with carbon compounds, and these experiments are typically performed with metal salts, and consequently they are of limited relevance to the carbon cycle. Liesegang diffusion also does not specifically produce circularly concentric patterns that destructively interfere as circular twins, nor do they form cavity structures (Figure 1a,b) [28]. Hence, while the Liesegang phenomenon has also been proposed to explain the periodic banding in malachite [29], the COR model explains much more elegantly the observed patterns and composition of botryoidal malachite [4]. Similarly, while the Liesegang diffusion phenomenon has long been invoked to explain the formation of patterns in agate geodes, there is little support for the Liesegang phenomena in agate geodes, which often contain organic matter and lack evidence for the diffusion of metal ions in silica gels [1].

Agate geodes are commonly believed to be formed through some interactions between heated fluids and volatiles associated with cavities in hot volcanic rocks [30]. Thermogravimetric analyses have shown that various volatile compounds are present in agate geodes, including NO, SO, CO₃²⁻, CH, and HF [31]. However, this method cannot detect macromolecular carbon, halogenated hydrocarbons, sulphurated hydrocarbons, nor halogens in trace concentrations. Other techniques such as optical microscopy have been used to demonstrate that some agate geodes are rich in bitumen, and that masses of opaque organic matter can be concentrated in the geometric centres of radiating acicular quartz inside botryoids [15]. Infrared spectroscopy has also been used to show the presence of alkanes, esters, ketones, and carboxylic acids organic matter from agate geodes, hinting at a biological origin [15]. Agate geodes are now widely known to contain organic matter, various hydrocarbon compounds, and disordered graphitic carbons [3]. Interestingly, ¹³C-depleted carbonate minerals are common in agate geodes [1,32], which may indicate an

origin from oxidised biomass. Furthermore, minerals such as calcite (Figures 3 and 4) and iron oxides or oxyhydroxides are almost ubiquitously found in agate geodes [3], whereas hydroxylated or water-bearing minerals and fluorite are also common, especially in geodes from acidic volcanic rocks [33]. Lastly, the oxygen isotope composition of agate is significantly more ^{18}O -enriched than their host volcanic rocks, which can be explained by the isotopic exchange with hydrothermal fluids or magmatically heated water [2]. However, biomass is also known to be ^{18}O -enriched [34], and carboxylic acids from decayed animals or plants could also have contributed to produce ^{18}O -enrichments in agate geodes. Hence, agate geodes contain various substances that indicate C-cycling through the oxidation of organic matter (either from biomass or abiotic synthesis) in aqueous solutions involving Fe, halogens, and other volatiles. In this light, observations in agate geodes and in Petri dishes with COR experiments need to be compared for different types of substances and self-similar patterns (Figure 5).

For concretions, there are two main growth processes proposed as models for the growth of carbonate concretions in the rock record: the cementation of diagenetic pore spaces by carbonate minerals and a displacive growth phenomenon, whereby diagenetic carbonate precipitation forces sedimentary layers apart [35]. It has also been suggested that concentric growth starts with the formation of an early diagenetic core nucleus in the concretion followed by the addition and precipitation of successive layers around the core [36]. Alternatively, an inverted growth model has further been proposed, whereby an outer rim of pyrite or carbonate first precipitates during diagenesis, followed by the radially inward growth of the concretion, with the concretion size controlled primarily by the availability of Fe [6,37]. While all these phenomena are not necessarily mutually exclusive, they do not explain nor predict the formation of specific geometric patterns commonly seen in concretions, including spheroidal, ellipsoidal, concentric, radial, irregularly rounded shapes, and the occurrence of fossils and organic matter within. Organic geochemical analyses have confirmed the presence of various residual molecular functional groups in kerogen from Toarcian organic shales and their limestone concretions, including carboxylic acids, aliphatics, ketones, phenols, and aromatics [38], as well as organic biomarkers such as pristane, phytane, and methylhopanes [11]. Organic matter in Lower Cambrian limestone concretions from the Niutitang Fm in south China have similar functional groups and have been considered in the COR model [5]. Lastly, Ediacaran concretions with circularly concentric pyrite layers have a sulphur isotope range of 25‰ with positive values up to +40‰, which suggest both microbial and abiotic processes of isotope fractionation [39]. Hence, it can be inferred that decarboxylation during the decomposition of biomass does not prevent the preservation of carboxylic acid functional groups in residual organic matter found associated with concretions.

Fossils and organic matter are commonly found in carbonate concretions (Figure 1c,d) and such observations suggest that organic matter, or specific compounds in biomass, participate in the abiotic reactions that produce concretions, and that these involved oxidation–reduction reactions of carbon compounds. Evidence of microbial activity in the formation of concretions is suggested by their abundance and patterns in modern and Phanerozoic concretions, where metabolically diverse microbes play a role in the decomposition of biomass [11]. Many concretions contain ^{13}C -depleted carbonate, which is consistent with the idea that some carbonate carbon originated from biomass (e.g., [6]). However, some concretions preserve evidence for methanogenesis during diagenesis, which has been inferred from ^{13}C -enriched carbonate in fossiliferous concretions from the Carboniferous [7,8]. In fact, evidence from organic matter is usually attributed to organic decay, primarily by invoking heterotrophic microorganisms [8]. Hence, microbial sulphate reduction most likely played a role in the production of sulphide minerals inside concretions, which has been based both on large ranges of ^{34}S -depleted pyrite related to microbial sulphate reduction in non-limiting sulphate concentration and on large ranges of ^{34}S -enriched pyrite related to microbial sulphate reduction under low concentrations of residual pore water sulphate [7,39]. These observations thus suggest that the mechanism of the formation

of concretions is linked to the diagenetic cycles of C, S, and Fe and specifically during the decomposition of biomass. Yet again, however, these inferred microbial processes do not reliably predict why concretions should have any geometric patterns (Figure 5, right column).

5.2. The Patterns and Substances of COR in Agate Geodes and Concretions

COR experiments show the same kinds of patterns and several overlapping compositional similarities with those in agate geodes and concretions. The similar patterns include spot proliferations, circular concentricity, twins, cavity structures, colour gradients, and radiations (Figure 5, left column). Spot proliferation begins at the microscopic scale and can also be seen as millimetric spots in agate geodes and as centimetric to decimetric cherty limestone concretions. Circular concentricity is also represented at microscopic to decimetric scales in all these objects. Spheroidal twins uniquely characterize circularly concentric spots, and they form cavity structures over the same range of size magnitudes. Also, each chemical wave in COR exhibits a colour gradient that can vary in length, which is also observed at microscopic and macroscopic scales in agate geodes and concretions. The summative Figure 5 remains incomplete, however, because there are other patterns produced by COR that are not represented here in any of the objects such as spirals, equidistant to branching lines, asymmetries, knobby or stromatolitic laminations, arborescences, and inversions. Hence, the COR model remains to be tested further on those patterns and on the substances involved in the reactions.

Now, the substances of agate geodes and concretions need to be compared with those of COR. The observations from agate geodes and concretions collectively suggest a role for redox reactions involving C and Fe in the formation of agate geodes and concretions and possibly also a role for halogens and S compounds. It is therefore natural to propose a significant role for the COR model in the formation of these objects, as it predicts that the underlying reactions should be abiotic, spontaneous, out-of-equilibrium, and produce fractal patterns. Observations of bubbles in the COR can be directly linked to the production of CO₂ during decarboxylation reactions, and in agate geodes, the unambiguous analogue is represented by micron-sized calcite inclusions in quartz, moganite, and cristobalite (Figures 3 and 4). In limestone concretions, comparisons can be made with the carbonate minerals that compose these objects formed around fossils of carbonate–apatite (e.g., Figure 1d) or of pyrite–haematite (e.g., Figure 1c,f). These compositions (Figure 5) are inferred based on Raman spectra as well as mineral colour, lustre, habit, and petrological context, and they are accompanied by zones of variable concentrations of organic matter. This is seen as brown to dark grey colour gradients in concretions and agate geodes, where these occur as concentrated disseminations of kerogen, in part, composing the circularly concentric waves described above. Fe-based catalysts in COR also analogously occur in agate geodes as ferruginous laminated cavity structures in red-coloured haematitic limestone, as haematitic fossils in limestone concretions, and as concentric pyrite rims in chert concretions. Hence, several substances representing the organic–carbonate and ferric–ferrous redox couples are directly linked through the substances of COR, agate geodes, and concretions.

For the immobilization of chemical waves, the variety of substances that can be involved in COR needs to be considered. Gels of N-isopropylacrylamide and polyacrylamide-silica gel composites have been used with success to immobilize chemical waves from the B–Z reaction [40], which suggests that colloidal silica and carbonate micrite play the same role, although this awaits further investigation. However, pattern formation from acidic COR does take place in alkaline solutions with colloidal silica [5]. Experiments have shown that COR can take place and produce patterns under a large range of reactant concentrations: 0.15–2.0 M H₂SO₄, 0.075–0.4 M NaBrO₃, and 0.05–0.8 M malonic acid [16,41,42]. In fact, there are also various other organic acids that can be used for COR, including carbonic acid, mono- and di-carboxylic acids, and ketones [16,17]. Similarly, COR are also known to produce patterns with various kinds of other strong oxidizers such as chlorate,

bromate, iodate, and hydrogen peroxide [43]. Various strong acids have also been used like hypophosphite, arsenate, and sulfuric acid, and various metal catalysts have been used to successfully produce COR patterns, including Mn^{2+} , Ce^{3+} , Fe^{2+} , Ru^{2+} , Cr^{2+} , Co^{2+} , and $\text{Fe}(\text{phen})_3^{2+}$ (ferroin), and $\text{Ru}(\text{bpy})_3^{2+}$ (ruthenium) [16,17]. While no sufficiently detailed visually correlated geochemical analyses were performed on the agate geodes to detect halogens, specific metals, or volatile elements, micro-Raman analyses revealed the presence of anatase and an unknown phase with peaks at 632 and 574 cm^{-1} , a bandwidth usually for metal–oxide bond vibrations. It remains unclear whether these minerals could have played some catalytic role along with Fe. Halogen elements like Cl, Br, and I all have high reactivity with carboxylic groups in organic matter under standard conditions and, in nature, they can become concentrated in evaporitic, volcanic, or diagenetic environments. While redox-sensitive elements like Fe are common in both volcanic and sedimentary environments, organic matter is particularly concentrated by life and is more abundant in sediments compared to volcanic rocks, which is perhaps the reason why concretions are far more common than agate geodes in the rock record.

In experiments, chemical waves are varied due the chaotic distribution, period, amplitude of oxidation spots, and colour gradients [4]. In fact, the accompanying oscillations of spots, zebra-stripes, fingerprint-like, grape-like, and turbinate columnar patterns remain unexplained. The oxidation spots develop as malonic acid, the only source of carbon in the experiment, which is oxidized to produce CO_2 (which accumulates in progressively larger bubbles), expected to produce halogenated organic acid intermediates. The ferroin redox indicator is red when reduced and blue when oxidized [16], such that this compound or other metal-bearing catalysts participate in the electron-transfer chain and the blue chemical waves must represent the reaction products and intermediates that diffuse radially from oxidation spots. In agate geodes, gradients of Fe-oxides occur as circularly concentric waves and/or Fe-bearing minerals with variable Fe-oxidation states visible with colour gradients of brown–orange, orange–yellow, and yellow–green accessory minerals and phases (Figure 1a,b). Twinned circular patterns of red haematite disseminations in chert from Paleoproterozoic botryoids [22] and the common presence of dispersed iron oxide minerals in agate geodes [1,3] further support the proposed catalytic role for iron in the abiotic formation mechanism. They exhibit the same kind of self-similar patterns with a chaotic distribution and variably sized oxidations spots, from tens of micrometres to decimetres (e.g., Figures 1a and 3a).

The production of CO_2 bubbles during COR arises in part from the cleavage of carboxyl functional groups from malonate through nucleophilic attacks via bromide (Br^-). Halogen elements are known to strongly interact with organic molecules and especially react to decarboxylate carboxyl groups. As carbon dioxide can precipitate carbonates at equilibrium under various slightly alkaline pH, for as long as divalent cations are available in residual diagenetic pore water solutions, CO_2 can precipitate corresponding carbonate minerals. In the experiments shown in Figure 2a–e, the circularly concentric patterns and the radially aligned quartz crystal converge towards a geometric centre where organic matter is concentrated, which is another key evidence that supports the interpretation of the diagenetic oxidation of organic matter. Not only are the compositions and patterns closely comparable between COR and agate geodes, but occurrences of micron-sized calcite in the Lyall geode (Figure 3c) and of micron-sized dolomite and calcite in the agate geode (Figure 4c,f) remarkably match with the random distribution of CO_2 bubbles in the COR experiments, all of which are also closely associated with the circularly concentric patterns (Figure 2e (rightmost panel), Figures 3c and 4b). Hence, the co-occurrence in agate geodes of the same kind of self-similar patterns composed of organic matter located in the geometric centre or forming gradients of dissemination in circularly concentric and twinning waves provide incontrovertible evidence for the oxidation of organic matter during geode formation and for the relevance of COR and carbon cycling in the origin of their patterns.

5.3. Pattern-Forming COR during Prebiotic Carbon Cycling and for Exobiology

Biochemical metabolisms are driven by electron transfer between an electron donor and acceptor molecules. During respiration, many molecular intermediates in metabolism include carboxylic acids, and the carboxyl functional group is often the locus of chemical reactions. Bromine, iodine, and chlorine are all essential trace elements for animals and many microorganisms, although their exact biochemical functions in the nervous, endocrine, and immune systems are not fully elucidated. However, many patterns made by metazoans adopt morphologies geometrically like those observed in COR [44]. Hence, there also exists a connection between COR and metabolic biochemistry, which has led to an abiotic model for pattern-forming abiotic carbon metabolism.

For instance, aerobic heterotrophy often involves glycolysis, which converts glucose to pyruvate. Pyruvate (an α -keto acid) can subsequently enter the tricarboxylic acid cycle (TCA cycle) during which decarboxylation occurs, which yields both energy (i.e., ATP and NADH) and CO_2 in a cyclic fashion that repeats until the reactants are depleted. This is analogous to COR because in the TCA cycle: 1—electron transfers with redox changes occur, 2— CO_2 is produced during the decarboxylation of organic acids, 3—self-similar patterns spontaneously and randomly appear on metazoans, and 4—Fe or other cationic catalysts are involved in the auto-catalysis of the reaction, such that both the TCA cycle and COR express different versions of the same oscillatory process [44]. Hence, COR might explain the ‘vitality’ of life, whereby life-forms require electron donors and acceptors, and the spontaneous reactions work in concert to perpetuate characteristic cellular self-similar patterns until they run out of electron donors or electron acceptors. So, when the COR solution ultimately turns all blue at the end of every experiment, the system becomes starved of electron donors and/or of electron acceptors and terminates, dies, in a slurry of CO_2 bubbles and residual decayed organic acids.

A COR scenario for the origin of life in hydrothermal environments is consistent with the prebiotic-like environments inferred from agate geodes and concretions, with variable reactants derived from volcanism or evaporitic environmental conditions. The presence of abiotic or biological organic acids and the co-occurrence of redox-sensitive metalliferous minerals (especially those with iron) is also essential for prebiotic chemical synthesis and abiotic chemical reactions. The inference is that a combination of oscillatory reaction networks between Fe, C, S, and halogen-bearing compounds formed the agate geodes. The new observations show that different polymorphs of SiO_2 , namely quartz, moganite, and cristobalite compose the matrix (Figures 3 and 4). The precursor colloidal silica, as an alkaline hydrated-gel substance, was reorganised by the way in which the circularly concentric waves of reaction products and intermediates were radially diffusing. In volcanically heated rocks, moganite is a mineral almost exclusively associated with quartz replacements, botryoidal habits, or geodes. In comparison, low cristobalite can form at temperatures around 570 K, which can be conducive to the evaporation of aqueous solutions and the consequent naturally concentrated ions of Fe^{2+} , SO_4^{2-} , carboxylic acids, halogens, and many other possible reactants, as suggested by experiments. Hence, spontaneous COR in volcanogenic environments with evaporating aqueous solutions could have resulted in the pockets of abiotically produced carboxylic acids to form patterns in colloidal silica, now preserved in SiO_2 polymorphs, that preserve circularly concentric gradients and cavity structures along with organic matter and Fe-oxide minerals. If this interpretation is correct, then agate geodes could be completely abiotic in origin.

Biosignatures are ‘possible’ signs of life, as objects, patterns, and/or substances [45]. Possible, because out of the large range of possible biosignatures, only a large number of independent observations can yield a solid biological interpretation. So, then, ‘abiotic biosignatures’ are those objects, patterns, or substances that arose from abiotic processes and that altered precursor-decomposed biomass. If the organic matter is biological in origin, then stable isotope compositions are predicted to record microbial metabolic fractionations. On the other hand, if the organic matter is demonstrably abiotic in origin, then the diagenetic spheroid objects should be considered an abiotic signature of carbon cycling, possibly

of prebiotic-like origin [43]. Hence, the expression ‘abiotic biosignature’ is not contradictory, and rather, it is expected to be widely applicable because diagenetic processes include both biological and abiotic reactions.

In summary, diagenetic spheroids are abiotic biosignatures or abiotic signatures of carbon cycling. It is important to emphasize that agate geodes and some types of concretions might be completely abiotic in origin if the organic acids used during diagenetic COR were abiotic in origin. This can happen in volcanic settings where abiotic carboxylic acids are synthesized from Fischer–Tropsch-type reactions, for instance during the hydrothermal circulation of carbonic fluids in mafic crust. For instance, the possibility of carboxylic acid oxidation by Fe-compounds could explain the highly similar botryoidal patterns in amygdules from Archean Beasley River Basalt [46]. While these were argued to represent fossilised raindrop patterns, the similarity of their patterns with those of COR (Figure 2a–e) rather suggest that organic matter and/or Fe-minerals should occur in those laminations. In any case, agate geodes most often come from volcanic environments, and, on Mars, haematite concretions are most likely abiotic in origin. This is because their formation on Mars would have involved volcanogenic and evaporitic concentrations of sulphate, halogens, and carboxylic acids, as have been detected in Martian soils [47]. In summary, the COR model elegantly explains why metazoan fossils are preserved inside diagenetic spheroids and how these diagenetic spheroids formed abiotically and under a range of diagenetic conditions, during the decomposition and decarboxylation of organic acids.

For exobiology, agate geodes and concretions should be recognized as sedimentological evidence of abiotic carbon cycling and the spontaneous oxidation of carboxylic acids in diagenetic conditions with saline solutions with also iron and sulphate. This leads to the recognition of fossil-bearing diagenetic spheroids as abiotic biosignatures from decomposed biomass and agate geodes as prebiotic-like abiotic signatures. Future systematic documentation of $\delta^{13}\text{C}_{\text{org}}$ and other biosignatures in agate geodes will reveal whether biological sources of organic molecules are common in these objects.

6. Conclusions

New petrographic and organic geochemical evidence shows patterns inside agate geodes and fossiliferous concretions. There is a striking similarity of patterns and substances involved in both objects and COR in Petri dishes. The new microscopy data from two agate geodes, combined with observations from other selected geodes and concretions, reveal at least six types of characteristic patterns within these objects and also in COR. Both agate geodes and concretionary-like objects can have rounded, circularly concentric equidistant laminations of a specific mineral assemblage, as well as laminations of ferric and ferrous iron minerals and/or organic matter, and these patterns span size scales from tens of micrometres to metres. In botryoidal habits inside agate geodes, spot proliferation and circularly concentric waves can be understood to have expanded radially to destructively interfere and produce circularly twinned patterns that form cavity-like structures and have colour-gradient patterns, all geometrically controlled and composed of disseminated organic matter, carbonate, and ferruginous substances (Figure 5). The preservation of fine geometric details in SiO_2 polymorphs is consistent with a volcanically heated and evaporative ionic solutions, that possibly included abiotically synthesized carboxylic acids. Biosignatures beyond the occurrence of organic matter remain to be identified in agate geodes; however, it is also possible that they preserve stable isotope evidence for microbial metabolism or further evidence for an origin as a purely abiotic chemical garden such as dendritic growths or abiotic biomorphs.

Concretions are often ‘tombs’ for metazoans, and they can also be inferred to have formed during the decomposition and diagenetic oxidation of organic acids. Co-produced carbon dioxide is in equilibrium with carbonate and bicarbonate and can ultimately precipitate as various carbonate minerals associated with these patterns, depending on the availability of divalent cations. Hence, concretions can serve as abiotic biosignatures. Compared with the prebiotic carbon cycle, COR also involve sustained reaction networks under

out-of-equilibrium conditions, the net production of energy through diffusion and electron transport chains, abiotic proto-electron transport chains, the generation of self-similar patterns, and the oxidation of Fe and carboxylic acid along with the production of haematite and CO₂. The COR model is thus also applicable for a key step in the origin of life [44] and becomes part of a temporal and spatial continuum of fractal patterns in nature. This now establishes broad correlations of objects with multiple scales of self-similar patterns and size, evolving where similar types of substances occur as reactants and over various timescales, including pre-life and prebiotic chemistry, life and biochemistry, and lastly, post-life and taphonomy.

Various hypotheses and opportunities for research emerge to rigorously test this new COR model, such as more broadly and systematically mapping organic matter and Fe-oxides in mineral assemblages from a wider range of concretions, agate geodes, and other diagenetic spheroids. Approaches to test the COR model in biochemistry could include molecular physiology with studies on the bodily distribution of diverse carboxylic acids and their relative concentrations in patterned tissues of metazoan as well as mapping gene expression to establish possible correlations with these patterns. Richer possibilities emerge from this new knowledge that might also lead to a better understanding of deleterious human health problems such as kidney stones, which also contain COR-like patterns [48]. Knowing more exactly the cause of such a medical condition could more easily lead to better treatments and more comfortable human lives. In fact, it is here predicted that COR will eventually become a broadly accepted theory, widely applicable in nature and indeed to explain the origin of various enigmatic natural spheroidal objects, and which requires much closer considerations in many disciplines of the natural sciences including in palaeontology, sedimentology, mineralogy, petrology, inorganic and organic geochemistry, prebiotic chemistry, biochemistry, developmental biology, human health, and biosignature studies in exobiology. The future of the COR model in nature is promising and bright.

Funding: This research received no external funding.

Data Availability Statement: All the data relevant to this paper are included herein or in the references.

Acknowledgments: I acknowledge constructive discussions with Z. She, R. Hazen, K. Devine, and N. Lane. Creators of the ruff project are thanked for their open access database, which was used to compare spectra obtained in this work. J. Götze is thanked for discussions on geodes and for co-editing this Special Issue.

Conflicts of Interest: The author declares no conflicts of interest.

References

1. Moxon, T.; Palyanova, G. Agate genesis: A continuing enigma. *Minerals* **2020**, *10*, 953. [[CrossRef](#)]
2. Götze, J. Agate fascination between legend and science. In *Agates III*; Bode Verlag: Lauenstein, Germany, 2011; pp. 19–133.
3. Götze, J.; Möckel, R.; Pan, Y. Mineralogy, geochemistry and genesis of agate—A review. *Minerals* **2020**, *10*, 1037. [[CrossRef](#)]
4. Papineau, D. Chemically oscillating reactions in the formation of botryoidal malachite. *Am. Min.* **2020**, *105*, 447–454. [[CrossRef](#)]
5. Papineau, D.; Yin, J.; Devine, K.; Liu, D.; She, Z. Chemically oscillating reactions during the diagenetic formation of Ediacaran siliceous and carbonate botryoids. *Minerals* **2021**, *11*, 1060. [[CrossRef](#)]
6. Coleman, M.L. Microbial processes: Controls on the shape and composition of carbonate concretions. *Mar. Geol.* **1993**, *113*, 127–140. [[CrossRef](#)]
7. Curtis, C.D.; Coleman, M.L.; Love, L.G. Pore water evolution during sediment burial from isotopic and minerals chemistry of calcite, dolomite and siderite concretions. *Geochim. Cosmochim. Acta* **1986**, *50*, 2321–2334. [[CrossRef](#)]
8. Cotroneo, S.; Schiffbauer, J.D.; McCoy, V.E.; Wortmann, U.G.; Darroch, S.A.F.; Peng, Y.; Laflamme, M. A new model of the formation of Pennsylvanian iron carbonate concretions hosting exceptional soft-bodied fossils in Mazon Creek, Illinois. *Geobiology* **2015**, *14*, 543–555. [[CrossRef](#)] [[PubMed](#)]
9. Seilacher, A. Concretion morphologies reflecting diagenetic and epigenetic pathways. *Sed. Geol.* **2001**, *143*, 41–57. [[CrossRef](#)]
10. Hennessy, J.; Knauth, P. Isotopic variations in dolomite concretions from the Monterey Formation, California. *J. Sed. Petrol.* **1985**, *55*, 120–130.
11. Plet, C.; Grice, K.; Pages, A.; Ruebsam, W.; Coolen, M.J.L.; Schwark, L. Microbially-mediated fossil-bearing carbonate concretions and their significance for palaeoenvironmental reconstructions: A multi-proxy organic and inorganic geochemical appraisal. *Chem. Geol.* **2016**, *426*, 95–108. [[CrossRef](#)]

12. Dodd, M.S.; Papineau, D.; Grenne, T.; Slack, J.F.; Rittner, M.; Pirajno, F.; O'Neil, J.; Little, C.T.S. Evidence for early life in Earth's oldest hydrothermal vent precipitates. *Nature* **2017**, *543*, 60–64. [[CrossRef](#)] [[PubMed](#)]
13. Papineau, D.; Dodd, M.S.; She, Z.; Iacoviello, F.; Slack, J.; Hauri, E.; Shearing, P.; Little, C.S. Metabolically diverse primordial microbial communities in Earth's oldest seafloor-hydrothermal jasper. *Sci. Adv.* **2022**, *13*, e2296. [[CrossRef](#)]
14. Svetova, E.N.; Cahzhengina, S.Y.; Stepanova, A.V.; Svetov, S.A. Black agates from Paleoproterozoic pillow lavas (Oneiga Basin, Karelian Craton, NW Russia): Mineralogy and proposed origin. *Minerals* **2021**, *11*, 918. [[CrossRef](#)]
15. Gaweda, A.; Rzymelka, J.A. "Bituminous agates" from rhyolites in the environs of Nowy Kosciól, Lower Silesia. *Mineral. Pol.* **1992**, *23*, 73–84.
16. Belmonte, A.; Ouyang, Q.; Flesselles, J.-M. Experimental survey of spiral dynamics in the Belousov-Zhabotinsky reaction. *J. Phys. II* **1997**, *7*, 1425–1468. [[CrossRef](#)]
17. Orbán, M.; Kurin-Csörgei, K.; Zhabotinsky, A.M.; Epstein, I.R. A new chemical system for studying pattern formation" Bromate-hypophosphite-acetone-dual catalyst. *Faraday Discuss.* **2001**, *120*, 11–19. [[CrossRef](#)]
18. Zaikin, A.N.; Zhabotinsky, A.M. Concentration wave propagation in two-dimensional liquid phase self-oscillating system. *Nature* **1970**, *225*, 535–537. [[CrossRef](#)]
19. Berner, R.A. Calcium carbonate concretions formed by the decomposition of organic matter. *Science* **1968**, *159*, 195–198. [[CrossRef](#)]
20. Canfield, D.E.; Raiswell, R. The evolution of the sulfur cycle. *Am. J. Sci.* **1999**, *299*, 697–723. [[CrossRef](#)]
21. Varkouhi, S.; Papineau, D. Silica botryoids from chemically oscillating reactions and as Precambrian environmental proxies. *Geology* **2023**, *51*, 683–687. [[CrossRef](#)]
22. Varkouhi, S.; Papineau, D.; Guo, Z. Botryoidal quartz as an abiotic signature in Palaeoarchean cherts of the Pilbara Supergroup, Western Australia. *Precamb. Res.* **2022**, *383*, 106876. [[CrossRef](#)]
23. Doyon, M.; Valiquette, G. *Roches Magmatiques du Centre-Nord de la Gaspésie*; ET 90-03; Energie et Ressources Naturelles du Québec, Gouvernement du Québec: Québec, QC, Canada, 1991; p. 78.
24. Heaney, P.; Davis, A.M. Observation and origin of self-organized textures in agates. *Science* **1995**, *269*, 1562–1565. [[CrossRef](#)] [[PubMed](#)]
25. Heaney, P. A proposed mechanism for the growth of chalcedony. *Contrib. Mineral. Petrol.* **1993**, *115*, 66–74. [[CrossRef](#)]
26. Threlfall, T. Structural and thermodynamic explanations of Ostwald's Rule. *Org. Process Res. Dev.* **2003**, *7*, 1017–1027. [[CrossRef](#)]
27. Toramaru, A.; Harada, T.; Okamura, T. Experimental pattern transitions in a Liesegang system. *Phys. D* **2003**, *183*, 133–140. [[CrossRef](#)]
28. Nabika, H.; Itatani, M.; Lagzi, I. Pattern formation in precipitation reactions: The Liesegang phenomenon. *Langmuir* **2020**, *36*, 481–497. [[CrossRef](#)]
29. Hartmann, R.J.; Kanning, E.W.; Klee, F.G. The Liesegang phenomenon applied to banded malachite. *J. Chem. Educ.* **1934**, *11*, 346–350. [[CrossRef](#)]
30. Smithsonian Institution, *Visitor Information Card about Agate Geodes*; Smithsonian National Museum of Natural History: Washington, DC, USA, 2017.
31. Richter-Feig, J.; Möckel, R.; Götze, J.; Heide, G. Investigation of fluids in macrocrystalline and microcrystalline quartz in agate using thermogravimetry-mass-spectrometry. *Minerals* **2018**, *8*, 72. [[CrossRef](#)]
32. Götze, J.; Möckel, R.; Vennemann, T.; Müller, A. Origin and Geochemistry of agate in Permian volcanic rocks of the Sub-Erzgebirge basin, Saxony (Germany). *Chem. Geol.* **2016**, *428*, 77–91. [[CrossRef](#)]
33. Götze, J.; Schrön, W.; Möckel, R.; Heide, K. The role of fluids in the formation of agates. *Chem. Erde* **2012**, *72*, 283–286. [[CrossRef](#)]
34. Tartèse, R.; Chaussidon, M.; Gurenko, A.; Delarue, F.; Robert, F. Oxygen isotope analysis of fossil organic matter by secondary ion mass spectrometry. *Geochim. Cosmochim. Acta* **2016**, *182*, 24–39. [[CrossRef](#)]
35. Sellés-Martinez, J. Concretion morphology, classification and genesis. *Earth Sci. Rev.* **1996**, *41*, 177–210. [[CrossRef](#)]
36. Oertel, G.; Curtis, C.D. Clay-ironstone concretion preserving fabrics due to progressive compaction. *Geol. Soc. Am. Bull.* **1972**, *83*, 2597–2606. [[CrossRef](#)]
37. Coleman, M.L.; Raiswell, R. Source of carbonate and origin of zonation in Pyritiferous carbonate concretions: Evaluation of a dynamic model. *Am. J. Sci.* **1995**, *295*, 282–308. [[CrossRef](#)]
38. Bernard, S.; Horsfield, B.; Schulz, H.-M.; Wirth, R.; Schreiber, A.; Sherwood, N. Geochemical evolution of organic-rich shales with increasing maturity: A STXM and TEM study of the Posidonia Shale (Lower Toarcian, northern Germany). *Mar. Petrol. Geol.* **2012**, *31*, 70–89. [[CrossRef](#)]
39. Xiao, S.; Schiffbauer, J.D.; McFadden, K.A.; Hunter, J. Petrographic and SIMS pyrite sulfur isotope analyses of Ediacaran chert nodules: Implications for microbial processes in pyrite rim formation, silicification, and exceptional fossil preservation. *Earth Planet. Sci. Lett.* **2010**, *297*, 481–495. [[CrossRef](#)]
40. Chou Chen, I.; Kuksenok, O.; Yashin, V.V.; Moslin, R.M.; Balazs, A.C.; Van Vliet, K.J. Shape- and size-dependent patterns in self-oscillating polymer gels. *Soft Matter* **2011**, *7*, 3141–3146. [[CrossRef](#)]
41. Körös, E.; Orbán, M. Uncatalysed oscillatory chemical reactions. *Nature* **1978**, *273*, 371–372. [[CrossRef](#)]
42. Agladze, K.I.; Krinsky, V.I.; Pertsov, A.M. Chaos in the non-stirred Belousov-Zhabotinsky reaction is induced by interaction of waves and stationary dissipative structures. *Nature* **1984**, *308*, 834–835. [[CrossRef](#)]
43. Epstein, I.R.; Kustin, K.; De Kepper, P.; Orbán, M. Oscillating chemical reactions. *Sci. Am.* **1983**, *248*, 112–123. [[CrossRef](#)]

44. Papineau, D.; Devine, K.; Albuquerque Nogueira, B. Self-similar patterns from abiotic decarboxylation metabolism through chemically oscillating reactions: A prebiotic model for the origin of life. *Life* **2023**, *13*, 551. [[CrossRef](#)] [[PubMed](#)]
45. Chan, M.A.; Hinman, N.W.; Potter-McIntyre, S.L.; Schubert, K.E.; Gillams, R.J.; Awramik, S.M.; Boston, P.J.; Bower, D.M.; Des Marais, D.J.; Farmer, J.D.; et al. Deciphering biosignatures in planetary contexts. *Astrobiology* **2019**, *19*, 1075–1102. [[CrossRef](#)] [[PubMed](#)]
46. Som, S.M.; Buick, R.; Hagadorn, J.W.; Blake, T.S.; Perreault, J.M.; Harnmeijer, J.P.; Catling, D.C. Earth's air pressure 2.7 billion years ago constrained to less than half of modern levels. *Nat. Geosci.* **2016**, *9*, 448–452. [[CrossRef](#)]
47. Eigenbrode, J.L.; Summons, R.E.; Steele, A.; Freissinet, C.; Millan, M.; Navarro-González, R.; Sutter, B.; McAdam, A.C.; Franz, H.B.; Glavin, D.P.; et al. Organic matter preserved in 3-billion-year-old mudstones at Gale Crater, Mars. *Science* **2018**, *360*, 1096–1101. [[CrossRef](#)] [[PubMed](#)]
48. Sigurava, M.; Saw, J.; Wilson, E.M.; Lieske, J.C.; Krambeck, A.E.; Williams, J.C.; Romero, M.F.; Fouke, K.W.; Curtis, M.W.; Kear-Scott, J.L.; et al. Human kidney stones: A natural record of universal biomineralization. *Nat. Rev. Urol.* **2021**, *18*, 404–432.

Disclaimer/Publisher's Note: The statements, opinions and data contained in all publications are solely those of the individual author(s) and contributor(s) and not of MDPI and/or the editor(s). MDPI and/or the editor(s) disclaim responsibility for any injury to people or property resulting from any ideas, methods, instructions or products referred to in the content.